Spin−Lattice Relaxation of the Phyllosemiquinone Radical of Photosystem I†

Yiannis Deligiannakis,* Jonathan Hanley, and A. William Rutherford

Section de Bioénergétique (URA CNRS 2096), Département de Biologie Cellulaire et Moléculaire, CEA Saclay, 91191 Gif-sur-Yvette, France

Received June 2, 1997; Revised Manuscript Received December 11, 1997

ABSTRACT: The spin−lattice relaxation time (T_1) of the phyllosemiquinone anion radical, A_1^-, of the photosystem I (PSI) reaction center, were measured between 4.5 and 85 K by electron spin−echo spectroscopy. The selective removal of the iron−sulfur centers, F_A, F_B, and F_X, from PSI allowed the measurement of the intrinsic T_1 of the A_1^- radical. The temperature dependence of the intrinsic $(T_1)^{-1}$ for A_1^- was found to be $\sim T^{1.3\pm0.1}$. The spin−lattice relaxation of the reduced form of iron−sulfur center F_X was also measured at low temperatures, in F_A/F_B-depleted PSI membranes. It was found that the fast-relaxing F_X center enhances the spin−lattice relaxation of the phyllosemiquinone due to dipolar coupling. The effect of the reduced forms of F_A/F_B on the T_1 of the phyllosemiquinone was minor compared to the effect of F_X. By analyzing the data with a dipolar model in the light of limitations imposed by other information present in the literature, the distance between the phyllosemiquinone and F_X in PSI is estimated to be 14.8 ± 4 Å.

Photosystem I (PSI)[1] is a large multi-subunit pigment−protein complex of approximately 300 kDa embedded in the photosynthetic membranes of plant algae and cyanobacteria. It comprises at least eleven different subunits and about 100 chlorophyll molecules (reviewed in ref 1). The redox components involved in the first steps of photoinduced electron transfer are located in the reaction center core complex, which is largely hydrophobic and comprises two homologous and probably pseudosymmetrical subunits PsaA and PsaB. Upon light excitation the primary electron donor, a pair of chlorophyll *a* molecules known as P700, forms a highly reducing singlet state which initiates charge separation between P700* and the proposed primary acceptor chlorophyll *a* (A_0). Electrons are then transferred to a molecule of phylloquinone, known as A_1, and subsequently through a series of three iron−sulfur centers before reaching soluble ferredoxin. The first iron−sulfur center reduced, F_X, is located at the interface between the PsaA and PsaB subunits at the stromal side of the complex. The other two iron−sulfur centers are within a peripheral subunit, PsaC, that is bound to the outer surface of the PsaA/PsaB complex (reviewed in refs 1 and 2).

The phylloquinone, A_1, functions as a one-electron carrier at a potential that is estimated to be lower than −700 mV (*2*). This unusually low potential makes this component of particular interest and it has been the focus of much research (reviewed in refs 2 and 3). However, the location of the phylloquinone has not yet been determined in the structural model obtained from X-ray diffraction studies of PSI crystals (*4*).

The study of the magnetic interaction between an organic radical and a metal can provide a direct estimation of the interspin distance (see refs 5 and 6 and references therein). In photosystem II, by using pulse EPR methods, several groups have estimated the distance between the fast relaxing metal centers and a range of organic free radicals involved in photosynthetic electron transfer (*7*−*15*). In the present work we have used this approach to study the magnetic interactions between the phyllosemiquinone radical and the iron−sulfur centers F_A, F_B, and F_X in PSI. From the spin−lattice relaxation of the phyllosemiquinone radical in the presence and absence of the iron−sulfur centers, the distances between the radical and the iron−sulfur center F_X, the dominant relaxer, was estimated.

MATERIALS AND METHODS

Liquid cultures of wild-type *Synechocystis* 6803 were grown in BG11 medium (*16*) to an OD (720 nm) of approximately 1.5 and were then harvested by centrifugation. The cells were broken by French press, and the cell debris was removed by further centrifugation. The isolated membranes were washed four times with ice-cold 20 mM Tricine, 5 mM EDTA, pH 7.8. After the final wash, they were resuspended to 2 mg/mL chlorophyll in 20 mM Tricine, pH 8.0, and frozen in liquid nitrogen.

A modified version of the method in (*17*) was used to remove the iron−sulfur centers F_A and F_B, without removing F_X. The membrane preparation was incubated at 20 °C in darkness in 7 M urea, 5 mM EDTA, 0.05% β-mercaptoethanol (v/v), 20 mM Tricine, pH 7.6, under a constant stream of argon. After 30 min of incubation the sample was diluted 5-fold in 20 mM Tricine, pH 7.8, and the PSI membranes

† Supported by Human Capital & Mobility Grant, Contract ERB0049GI1901, and a Human Frontiers Science Program Grant RG-349/94.

* Corresponding author.

[1] Abbreviations: PSI, photosystem I; A_0, primary electron acceptor chlorophyll *a*; A_1, the PSI phylloquinone secondary electron acceptor; cw EPR, continuous wave electron paramagnetic resonance; ESEEM, electron spin−echo envelope modulation; β-DM, *n*-dodecyl β-D-maltoside; F_A, F_B, and F_X, the three [4Fe-4S] centers of PSI; HEPES, *N*-2-hydroxyethylpiperazine-*N*′-2-ethanesulfonic acid; PsaA, -B, -C... are the polypeptides coded by the genes *psa*A, -B, -C..., respectively; Tricine, *N*-[2-hydroxy-1,1-bis(hydroxymethyl)ethyl]glycine.

S0006-2960(97)01297-X CCC: $15.00
Published on Web 02/18/1998

were isolated by ultracentrifugation. To obtain material lacking all three of the iron−sulfur centers (F_A, F_B, and F_X), the same procedure was used except β-mercaptoethanol was omitted and 1.5 mM $HgCl_2$ was present during the incubation with urea.

The semiquinone radical was generated using a procedure based on that of (*18*) using modifications described in (*19*). Briefly samples were illuminated (2 min at 200 K) in the presence of 25 mM sodium dithionite and 200 mM glycine, pH 10.0. This procedure results in the formation of approximately 30% of the phyllosemiquinone. This low yield was used in order to minimize the possibility of contamination from other radicals (*19*).

X-band EPR spectra were recorded at liquid helium temperatures with a Bruker ER 300 X-band spectrometer equipped with an Oxford Instruments cryostat. Pulsed EPR was performed with a Bruker ESP 380 spectrometer with a dielectric resonator, described in (*20*). Spin−lattice relaxation times, T_1, were measured by saturation−recovery at 9.6 GHz. The saturation recovery was monitored by recording the two-pulse echo intensity ($\pi/2$−120 ns−π; with $t_{\pi/2} = 16$ ns) as a function of the time after a saturating pulse sequence (*21*, *22*) in order to minimize contributions from spectral diffusion as described in (*15*). The pulse length was $t_p = 8$ ns corresponding to $H_1 \sim 10$G; typically $N = 40$ pulses with interpulse delay 0.4 μs were used. The repetition rate was adjusted in every measurement to ensure complete magnetization recovery.

The relaxation enhancement of a slowly relaxing spin by a fast relaxing spin was described by Bloembergen (*23*) and for a pairwise point−dipole interaction between two isotropic spins with T_{1f}, $T_{2f} \ll T_{1s}$ can be expressed as (*24*, *5*)

$$k_{1\theta} = \frac{\gamma_s^2 \mu_f^2}{r^6}\left\{ {}^1/_6 \underbrace{\frac{T_{2f}}{1+(\omega_s-\omega_f)^2 T_{2f}^2}(1-3\cos^2\theta)^2}_{B\text{ term}} + 3\underbrace{\frac{T_{1f}}{1+\omega_s^2 T_{1f}^2}\sin^2\theta\cos^2\theta}_{C\text{ term}} + {}^3/_2 \underbrace{\frac{T_{2f}}{1+(\omega_s+\omega_f)^2 T_{2f}^2}\sin^4\theta}_{E\text{ term}} \right\} \quad (1)$$

where "f" and "s" denote the fast and slow relaxing spins, respectively; γ_s is the magnetogyric ratio of the slowly relaxing spin, r is the interspin distance, ω_f and ω_s are the resonant frequencies, and θ is the angle between the interspin vector and the external magnetic field. The external magnetic field is taken as parallel to the z-axis of the laboratory frame. The observed spin−lattice relaxation rate is $k_1 = k_{1i} + k_{1\theta}$, where $k_{1i} = 1/T_{1i}$ and is the intrinsic spin−lattice relaxation rate of the slowly relaxing spin. The recovery trace is described by the equation (*6*, *11*)

$$f(t) = 1 - N\int_0^{\pi} \sin\theta\, e^{-k1t}\, d\theta$$

where N is a scaling factor.

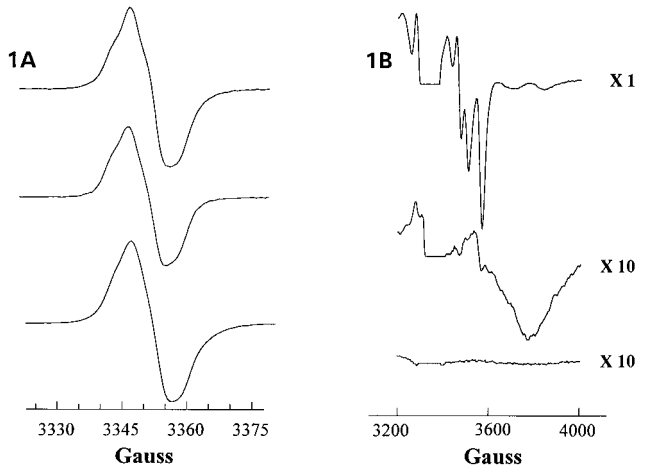

FIGURE 1: EPR spectra of reduced electron acceptors in PSI. (A) The phyllosemiquinone, A_1^-. Upper trace: A_1^- in the presence of reduced F_X^-, F_A^-, and F_B^-. Middle trace: A_1^- in the presence of reduced F_X. Lower trace: A_1^- in the absence of the iron−sulfur centers. EPR conditions: temperature 26 K; microwave power, 6.34 μW; 2G modulation amplitude. (B) Iron−sulfur spectra corresponding to the samples in (A) above. EPR conditions: temperature, 8 K; microwave power, 20 mW; 20G modulation amplitude. Samples were reduced by sodium dithionite and by illumination at 200 K as described in the methods.

For the estimation of the interaction distance from the dipolar enhancement, knowledge of the relaxation times of the fast relaxing spin, in our case the iron−sulfur center F_X, is required. In comparable earlier work on PSII (*11*, *13*−*15*) and bacterial reaction centers (*25*, *12*), the relaxation times of the fast relaxing spin (i.e., the acceptor-side nonheme iron) was not directly measured. However, in the present case the T_1 of the fast-relaxing iron−sulfur center F_X was measured directly, and this is used explicitly in the data analysis for estimating the T_2 and thereby the interspin distance (for a discussion on this point see also ref *26*). The approach used to estimate T_2 is explained in detail in the Results. For analysis of the data, we consider that, at the low temperatures of our experiments, the effective spin state of F_X is $S = {}^1/_2$ (*27*).

For the extraction of the dipolar rates from the data we need to know the orientation of the interspin vector F_X−A_1 relative to the principal axis system of the g_f tensor. In this case the g_f is the tensor of F_X and this orientation is unknown. However, the effect of the g_f anisotropy can be assessed so that reasonable approximations can be made and the range of possible distances evaluated. The approach used is given in detail in the Results (also see refs 28−30).

RESULTS

Figure 1A shows the X-band EPR spectra of the phyllosemiquinone, A_1^-, from PSI preparations in the following states: (1) A_1^- in the presence of the reduced form of F_X, F_A, and F_B, designated F_X^-, F_A^-, and F_B^- (Figure 1A upper trace); (2) A_1^- in the presence of F_X^- (Figure 1A, middle trace); and (3) A_1^- in the absence of the iron−sulfur proteins (Figure 1A, lower trace). The corresponding spectra from the iron−sulfur centers themselves are shown in Figure 1B. The phyllosemiquinone EPR spectrum is characterized in each case by $g = 2.0043 \pm 0.0002$ and $H = 9.8 \pm 0.3$ G with partially resolved hyperfine structure. These characteristics are typical of the phyllosemiquinone radical in PSI

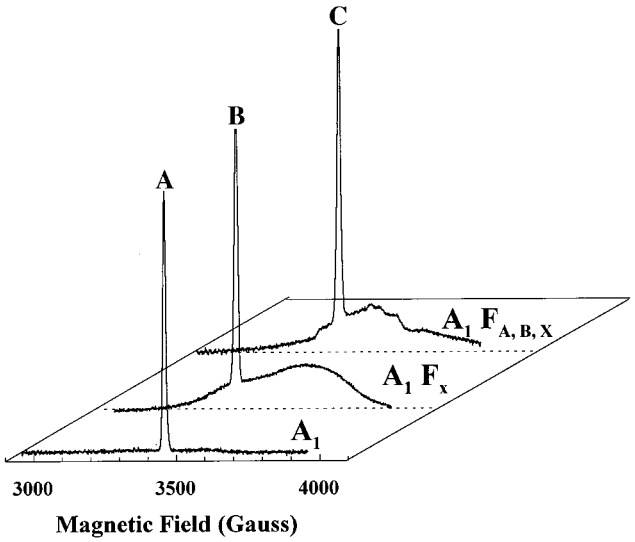

FIGURE 2: Field-swept echo spectra of reduced electron acceptors in PSI. The spectra represent the amplitude of the electron spin−echo resulting from a two-pulse sequence ($\pi/2-144$ ns$-\pi$, with $t_{\pi/2} = 16$ ns) as a function of the magnetic field. (A) A_1^- in the absence of the iron−sulfur centers; (B) A_1^- and F_X^-; (C) A_1^-, $F_A^-F_B^-$, and F_X^- . Experimental conditions: sample temperature, 8.2 K (A), 4.3 K (B), and 8.3 K (C); time interval between successive pulse sets, 40 ms; microwave frequency, 9.66 GHz.

(*18*). It is important to note that the poorly resolved hyperfine structure was present in all preparations, indicating no change to the local environment induced by the different biochemical preparations.

The spectra from the iron−sulfur centers in Figure 1B (upper trace) show typical features expected from PSI when all three iron−sulfurs were reduced (see ref 1 for a review). When F_X^- was present without F_A and F_B (Figure 1B, middle trace), its spectrum was broadened somewhat, as reported earlier in comparable material (*31*). The residual contamination of F_A^- and F_B^- in this preparation was less than 5%. The lower trace in Figure 1b shows the almost complete absence of iron−sulfur centers (<5% F_X^-) in this preparation.

Electron spin−echo-detected spectra and spin−lattice relaxation measurements were done on A_1^- and the iron−sulfur signals in the states shown in Figure 1. The echo-detected EPR spectrum of A_1^- in the absence of the iron−sulfur centers is shown in Figure 2A. In accordance with the cw EPR spectra, essentially no echo from the iron−sulfur centers was present (compare Figure 2C). The spin−lattice relaxation of the A_1^- was measured by monitoring the saturation recovery of the two-pulse echo at the field position $H = 3457$ gauss corresponding to the maximum absorption of A_1^-. A typical echo-detected saturation recovery curve of A_1^- at 4.5 K is shown in Figure 3. The recovery is well described by a single exponential with $T_1 = 62$ ms. The residual from the fit is shown at the bottom of the transient (Figure 3). The relaxation measurements were extended over the 4.5−85 K range; the observed spin−lattice relaxation rates were single exponential throughout this range. The temperature dependence of the spin−lattice relaxation rates determined in this way ($1/T_{1i} \sim T^{1.3\pm0.1}$) is shown in Figure 4 (filled circles).

The echo-detected EPR spectrum for F_X^- in the absence of the iron−sulfur centers F_A and F_B is shown in Figure 3B.

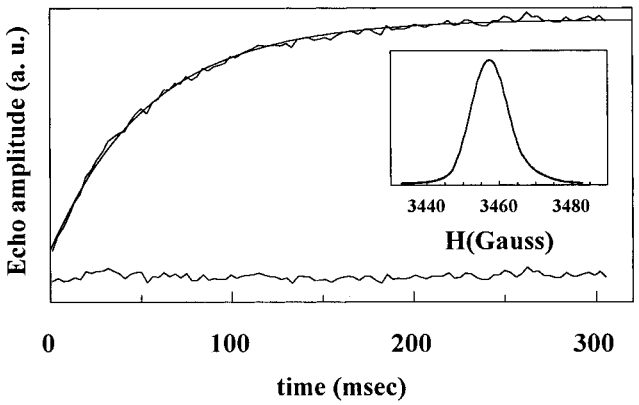

FIGURE 3: Saturation−recovery transient observed for the A_1^- in $F_A^-F_B^-$ and F_X^- -depleted PSI. The exponential fit is superimposed. The difference between the experimental and the fitted curve is shown at the bottom. Experimental conditions: sample temperature, 4.5 K; magnetic field, 3457 gauss; two-pulse repetition time, 400 ms.

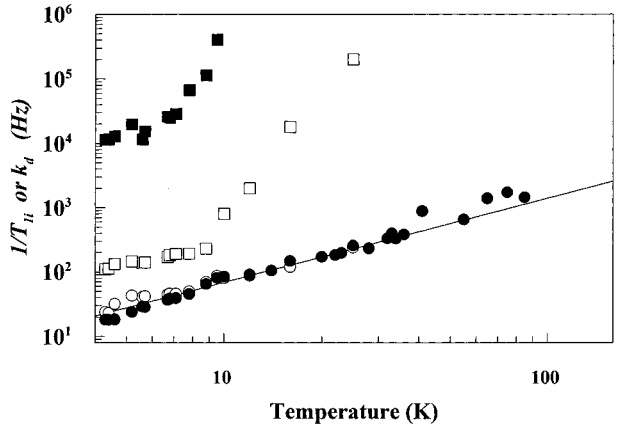

FIGURE 4: Temperature dependence of the intrinsic spin−lattice relaxation rate ($1/T_{1i}$) for A_1^- (●) in $F_A/F_B/F_X$-depleted and for F_X^- in F_A/F_B-depleted PSI (■). The scalar relaxation rare for the A_1^- in the presence of F_X^- is also shown (○). Temperature dependence of the dipolar enhancement rates k_{1d} for the A_1^- (□) estimated by using the B term of eq 1. The solid line is a fit of the function $1/T_{1i} \sim T^{1.3\pm0.1}$ to the data for the T_1 of A_1^-.

The broad F_X^- signal was detectable only at temperatures <10K and was broad even at 4.2K. In the field-swept spectrum of F_X (Figure 2B), its broad low-field features were better resolved than in the first-derivative cw EPR spectrum (Figure 1).

The T_1 of the F_X^- (see below) was isotropic (within 10%) across the spectrum. In addition the phase-memory time T_m (i.e., the two-pulse echo decay) across the spectrum was measured for F_X^-, and it was found to be essentially isotropic across the spectrum (data not shown); a typical value for T_m was about 0.8 μs at 4.6 K. In ESEEM measurements performed across the F_X^- spectrum, we detected essentially no nuclear modulations (data not shown). We conclude that the line shape of the F_X^- presented in Figure 2B is only minimally affected by the factors which potentially can distort the field-swept echo-detected EPR spectra, i.e., ESEEM or relaxation anisotropy (*32*).

Typical echo-detected saturation recoveries recorded across the EPR spectrum of F_X^- (Figure 2B) are presented in Figure 5. Panels b−d in Figure 5 show saturation recoveries at

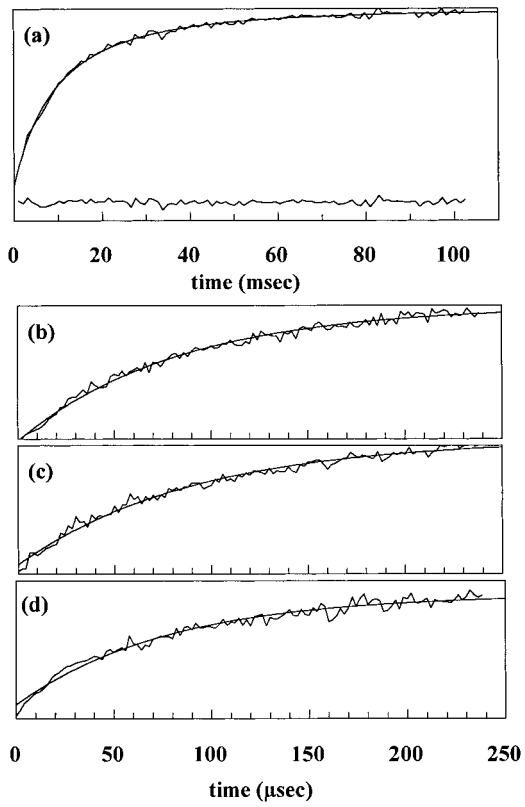

FIGURE 5: Saturation−recovery transient observed in F_A/F_B-depleted PSI at magnetic fields of 3720 G (b), 3440 G (c), and 3490 G (d). The exponential fit is superimposed. (a) Saturation recovery transient observed for A_1^- at $H = 3457$ G. The fit by using the *B* term of eq 1 is superimposed; the difference between the experimental and the fitted curve is shown at the bottom. Experimental conditions: sample temperature, 4.7 K; microwave frequency, 9.65 GHz; other experimental conditions as in Figure 2.

magnetic fields where only the F_X^- spins contribute to the detected echo (i.e., outside of the A_1^- signal). The recoveries were about 2 orders of magnitude faster than at the field position where the A_1^- spins are on resonance (i.e., $H =$ 3457 gauss, see Figure 5a). The F_X^- echo was detectable from 4.2 K up to about 10 K. At higher temperatures the phase-memory time precluded any F_X^- echo detection. Throughout this temperature range, the recovery for the F_X^- was single-exponential. The average spin−lattice relaxation rate, $1/T_{1F_X}$, for F_X estimated by a single-exponential fit is shown in Figure 4 (filled squares).

The echo-detected EPR spectrum for F_X^-, F_A^-, and F_B^- is shown in Figure 2C. Echo-detected saturation recoveries were not studied in detail because it became clear that F_X^- was the dominant relaxer for A_1^- (see below). For example, the T_1 for F_A^- and F_B^- at 6.7 K were estimated to be 7.4 ms, a value that is significantly slower than for F_X^- (<1 ms) at this temperature.

The saturation recovery for A_1^- in the presence of F_X^- was faster than for A_1^- alone and was not single-exponential in contrast to the situation for A_1^- alone (e.g., at 4.5 K the dipolar enhancement rate for A_1^- in the presence of F_X^- was $k_d = 106$ Hz). This is attributed to a dipolar interaction between F_X^- and A_1^-. When $F_A^-F_B^-$ are present, after taking into acount the contribution of their intrinsinc relaxation to the A_1 echo recovery, the dipolar enhancement of A_1^- was, within the experimental error of our measurements, similar in samples with and without $F_A^-F_B^-$ (not shown). This indicates that F_X^- is the dominant relaxer. However, because the echo recovery from the underlying F_A^- and F_B^- occurred in the time range of the enhanced A_1^- recovery, a detailed study and calculation was done on A_1^- relaxation in the presence of F_X^- alone.

The dipolar interaction between F_X^- and A_1^- can be described by eq 1, and given the relaxation times of the F_X^- that we measure here, the *B* term in eq 1 dominates. Thus we analyzed the data by using the *B* term of the dipolar model (eq 1), and the least-squares fit is superimposed on the experimental curve, Figure 5a. The dipolar rates k_d estimated by the fit at various temperatures are presented in Figure 4 (open squares). The scalar relaxation rates for the A_1^- extracted from the fits are also shown in Figure 4 (open circles). At temperatures above 10 K the dipolar rates increase due to the increase of the relaxation rate of F_X^- and this continues up to about 25 K where it appears to start to slow. On the basis of estimates of the T_1 of F_X^- from cw EPR line width data (*27*), it is expected that at this temperature the T_1 of F_X^- becomes very fast and starts to decouple from A_1^- (see eq 1).

Based on the dipolar enhancement of the relaxation A_1^- by F_X^-, using the *B* term of eq 1, it is possible to deduce the distance between A_1^- and F_X^-. In the *B* term of eq 1, the T_2 of F_X^- (T_{2f}) enters the calculation. We have estimated T_{2f} by using the following approach: (a) Above 10 K the line width of the F_X^- signal is determined by its T_1 as demonstrated in ref 27. This means that $T_1 = T_{2f}$ at these temperatures. This is verified by the experimental observation that the relaxation enhancement of A_1^- roughly parallels the temperature dependence of the T_1 for F_X. (b) As the temperature is lowered, the T_1 slows down and becomes slower than T_{2f}. Since under these conditions the T_{2f} is no longer determined by T_1, the T_{2f} becomes temperature independent. From the *B* term of eq 1, the dipolar-enhanced relaxation rate of A_1^- should now follow the T_{2f} trend. And indeed experimentally it is seen that at temperatures below 10 K the dipolar-enhanced relaxation rate of A_1^- becomes independent of temperature. The T_2 of F_X^- below 10 K has not been measured directly, however; at the crossover point of 10 K, it must be comparable to that of T_{1f} and since it is independent of temperature, this T_{2f} value applies to lower temperatures also. Thus the T_{2f} of F_X^- at 10 K and below can be taken as being equal to the T_1 of F_X^- at 10 K (i.e., 1.2 ± 0.3 μs).

A further estimation for the T_2 is provided by the analysis of the line width. In the analysis of Bertrant et al. (*27*), the T_2 is estimated to be 1−0.5 μs, a range that overlaps our estimate. To illustrate the influence of shorter T_2 values, we calculated the effect of using the faster limit of this approximation of T_2 (0.5 μs) in plot like that of Figure 6 (see below), and we found that although all the distance values increased, the increase is on the order of 1.4 Å. We consider, then, that at 10 K and below, our distance values are likely to be somewhat underestimated compared to the values obtained at higher temperatures where T_2 is determined by T_1 (see below).

To extract the distance parameter from the data, using the relation $\omega = g\beta H/\hbar$, the *B* term in eq 1 can be written as $(\gamma_s^2\mu_f^2/6r^6)g_s^2T_{2f}/[g_s^2 + \omega_s(g_s - \boldsymbol{g}^L_f)^2T_{2f}^2](1 - 3\cos^2\theta)^2$,

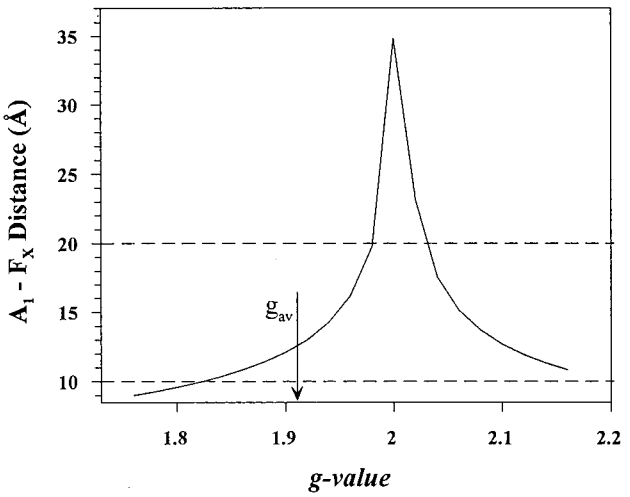

FIGURE 6: Plot of the effect of $\mathbf{g}_f$ on the calculated distance in the *B* term of eq 1 expressed as $k_{1\theta} = k_d(1-3\cos^2\theta)^2$, with k_d as defined in the text, when fitted to the data taken at 12 K. The T_{2f} value used was 1 μs (see text).

where $\mathbf{g}^{L}_f$ is the anisotropic $\mathbf{g}_f$ tensor expressed in the laboratory frame. $\mathbf{g}^{L}_f$ is calculated by standard procedures, i.e., by using rotation matrixes $\mathbf{g}^{L}_f = R^{-1}(u,w,v)\,\mathbf{g}^{P}_f\,R(u,w,v)$, where $\mathbf{g}^{P}_f$ is the $\mathbf{g}_f$ tensor in its principal axes system and *u*, *w*, *v* are the appropriate Euler angles relating the two-axis systems (see refs 28−30). However, the orientation of the *g* axes of F_X^- relative to the F_X-A_1 vector is unknown, so the appropriate $\mathbf{g}^{L}_f$ is also unknown. To assess the effect of the anisotropy of the $\mathbf{g}_f$ tensor, we have fitted our data using the *B* term, having the $F_X^-−A_1^-$ interspin distance *r* as the only adjustable parameter. We have performed these fits for a range of orientations, covering 30 representative sets of angles (*u*, *w*, *v*). With the exception of a small subset of angles, the F_X-A_1 distances obtained fell between 10 and 20 Å. The small subset of (*u*, *w*, *v*) values correspond to a $\mathbf{g}_f$ tensor oriented with its g_z axis making an angle of 40−45° with the interspin vector and give significantly longer interspin distances (20−29 Å). This situation corresponds to a very small fraction of the possible orientations, and therefore such longer distances are improbable.

In earlier studies involving a relaxer with *g* anisotropy, the g_{av} was used and the *B* term was used in the form $k_{1\theta} = k_d(1 - 3\cos^2\theta)^2$ with $k_d = (\gamma_s^2\mu_f^2/6r^6)g_s^2T_{2f}/[g_s^2 + \omega_s(g_s - g_f)^2T_{2f}^2]$ (*11*, *12*). In this expression the g_f is taken to be angle-independent, which for an anisotropic relaxer is not the case. The calculations in the previous paragraph showed empirically that for the present system the use of $g_f = g_{av}$ is a valid simplification, notwithstanding the small subset of (*u*, *w*, *v*) values giving significantly longer interspin distances. In what follows, we reiterate this argument in the context of the *B* term in the form $k_{1\theta} = k_d(1 - 3\cos^2\theta)^2$ addressing the effect of the g_f value directly.

To illustrate the effect of the g_f value we have used the full range of possible *g* values for F_X and have calculated their influence on the calculated interspin distance. Typical results for this series of calculations are shown in Figure 6 for $T = 12$ K. The figure shows how the distance for F_X-A_1 is influenced by g_f over the range relevant to F_X (g = 1.76−2.14). It is then clear that if the F_X-A_1 vector were oriented relative to the *g* axes of F_X in such a way that the g_f were 2, the calculated distance would be longer than 20 Å. It is also clear that with the exception of the narrow range of values around $g = 2$, the vast majority of other *g* values would give distances which fall within 10−20 Å. Now, the rhombic *g* tensor for F_X has principal values of $g_x = 2.14$, $g_y = 1.84$, and $g_z = 1.76$. In the $\mathbf{g}$ tensor principal axes system, a value of $g_f = 2$ occurs only in a narrow range of polar angles between 47 and 51°. From the expression of the *B* term, it can be seen that the dipolar enhancement is significant only for θ angles close to 90 or 0° while it is minimized for $\theta = 54.7°$. By simple geometric arguments, one can see that the polar angles 47−51° match the optimal θ angles (90° or 0°) for only a very limited range of Euler angles (*u*, *w*, *v*), i.e., when the g_z axis of F_X is close to 44° relative to the F_X-A_1 vector. This greatly limits the probability that the F_X-A_1 vector will be oriented relative to F_X in such a way that its g_f is 2. Furthermore, even in the exceptional case where the $g_f = 2$, the calculations by using the complete anisotropic tensor, as described in the previous paragraph, show that contributions from other *g* values will effectively shorten the calculated distance. Therefore the longer values for the F_X-A_1 distance are considered to be unlikely.

Overall the calculations and fits show that the distance estimations using an isotropic g_{av} (1.91), in which the dipolar rate k_d is the only fitting parameter, give distances that are in agreement with the distances calculated by using an anisotropic g_f tensor. It is therefore reasonable to simplify some of the data treatment by using the g_{av}. This simplification has proved valid and useful in previous studies (*11*, *12*).

By using the *B* term of eq 1 and the g_{av} as explained above, we have estimated an A_1-F_X distance at a range of temperatures using the appropriate T_{2f} values. Examples of the values obtained were the following: (a) at 10 K, 13.4 ± 2.2 Å; (b) above 10 K, 14.9 ± 2.3 Å; and (c) below 10 K, 14.2 ± 2.2 Å. Overall the distance information calculated for a series of temperatures provided a mean distance of 14.8 Å for $A_1^-−F_X^-$. When the errors from the approximations made for the *g* orientation described above were taken into account, we arrived at an A_1-F_X distance estimate of 14.8 ± 4.0 Å.

DISCUSSION

The spin−lattice relaxation properties of phyllosemiquinone anion radical (A_1^-) and the reduced iron−sulfur center F_X (F_X^-) in PSI have been investigated. By removal of the iron−sulfur centers it was possible to study the relaxation of F_X^- alone and the relaxation of A_1^- alone or in the presence of F_X^-.

The T_1 of F_X^- is short as expected from its cw EPR properties which showed it to be a much faster relaxing species than F_A^- and F_B^-. The $1/T_{1F_X}$ shows a steep temperature dependence which is weakly anisotropic across the spectrum. This weak anisotropy is consistent with an Orbach process (*34*), and such a process has already been shown to be the dominant process for relaxation of F_X^- (*27*). Analogous weakly anisotropic relaxation due to an Orbach process has been observed earlier in, for example, the iron−sulfur center of the ferredoxin of *S. maxima* (*35*).

The measured intrinsic spin−lattice relaxation of the A_1^- (i.e., in the absence of the iron−sulfur proteins) is slower than that of the plastoquinone radical Q_A^- and the tyrosine

radicals Y_D° and Y_Z° (*14*) of PSII. On the other hand the intrinsic relaxation rate of the A_1^- is rather similar in magnitude and in terms of its temperature dependence to those observed for other radicals in photosynthetic systems such as the cation radical of the bacteriochlorophyll special pair in *Rhodobacter sphaeroides* (*12*), a chlorophyll monomer cation in PSII (*14*) and the pheophytin anion in PSII (*15*). Since the A_1^- resonance line is broadened by hyperfine interaction (see e.g. Figure 2), we consider that the dominant spin−lattice relaxation mechanism is the modulation of the hyperfine interaction by the lattice vibrations (for a review, see ref 36 and references therein).

The A_1^- signal was studied in the presence of the iron−sulfur centers. Although the magnetic interaction between the rapidly relaxing F_X^- and A_1^- could not be detected as a change in the line shape of the cw EPR spectrum of the radical, it was found to decrease the spin−lattice relaxation time of the A_1^-. A quantitative estimation of the dipolar interaction between the two paramagnetic centers provides an estimate of the F_X^-−A_1^- distance as being 14.8 ± 4.0 Å.

The additional presence of F_A^- and F_B^- did not significantly alter the relaxation properties of the A_1^-, compared to the effect of F_X^- alone on the T_1 of A_1^-. However, measurements of the T_1 of F_A^- and F_B^- showed that the T_1 values of these centers were slow enough to contaminate relaxation kinetics measured for A_1^-. Therefore the detailed temperature study and the calculation of the distance were only done on material lacking F_A^- and F_B^-.

The validity of the F_X^- to A_1^- distance measurement depends on the assumption that A_1^- properties are not modified by the biochemical treatments used for the removal of the iron−sulfur centers in PSI. There are several indications that A_1^- is unperturbed by the treatments used. (1) The hyperfine structure of the cw EPR spectrum of A_1^- is present in all samples (see Figure 2). (2) The electron spin−echo envelope modulation (ESEEM) of A_1^- was identical in PSI where the iron−sulfur centers were removed (data not shown) and in the control PSI sample (*37*). (3) The similar temperature dependence of the spin−lattice relaxation of A_1^- before and after the removal of the iron−sulfur centers shows that the treatment for the selective removal of the iron−sulfur centers does not alter the coupling of the A_1^- spin with the lattice phonons. Overall, it seems clear that A_1^- and its immediate environment are unaltered by the treatments given in this work and therefore that the distance estimate is reliable.

The estimated A_1−F_X distance obtained from the dipolar magnetic interaction is close to the limit where exchange interactions are considered to be resolvable by EPR (see ref 38) and references therein) and indeed, F_X^- has no static interaction on the A_1^- signal detected by cw EPR. On the other hand, an effect of an exchange interaction on the scalar T_1 of the A_1^- would be $\sim JT_{2f}/(1 + (\omega_s - \omega_f)^2T_{2f}^2)$ (*24*) and its contribution would be detected as a faster scalar rate for A_1^-. In the present case the scalar rates of the A_1^- estimated from the fit to the experimental data (open circles in see Figure 5) are similar to the intrinsic rates of the A_1^- although a small acceleration in the rate is observed at nearly all the temperature points studied. Because of the small size of this effect, we are unable to affirm that this shift is significant; however, at face value the data could indicate the presence of an exchange interaction of a few gauss. If so, then the exchange interaction could be significant in terms of the electron-transfer reaction between these components.

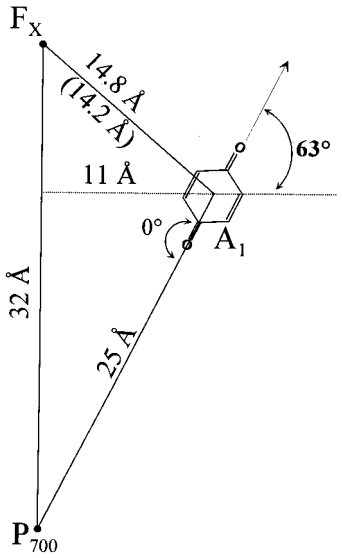

FIGURE 7: Scheme of the position of A_1 in PSI. The A_1−F_X distance 14.8 Å is from the present work, the value of 14.2 Åfor this vector. The 11 Å from the *C*2 axis is obtained from the P700−A_1 distance 25 Å (*43*), the 0°angle between the O−O axis and the P700−A_1 vector (*44*), and the 63° tilt of the O−O axis versus the membrane (*19*).

The estimate of 14.8 ± 4.0 Å for the distance between A_1 and F_X seems reasonable in the light of other estimates of this distance in the literature. From a kinetic study of electron transfer from A_1 to F_X and by application of model of Moser et al. (*39*) for electron transfer, Setif and Brettel (*40*) estimated the edge to edge distance between A_1 and F_X to be 10.7 Å. Given the estimates made for the effective radii of F_X (4.86 Å) and A_1 (2.84 Å), the center to center distance based on electron-transfer then becomes 18.4 Å. This value is considered to be an overestimation and should be considered as an upper limit (*40*). In a separate study, an edge to edge distance of 7 Å (center to center 14.7 Å) was obtained also based on the kinetics of A_1 but using a different electron-transfer model (*41*; see also Brettel (*2*) for a discussion of these estimates). Both of these two estimates fit with the distance deduced from the dipolar coupling reported here since it is considered to be a center to center distance.

Photovoltage measurements in PSI suggested that electron transfer from A_1 to F_X constituted 22% of the voltage generated from P700 to F_X (*42*). This translates to transmembrane separation of 7 Å (based on a P700 to F_X distance of 32 Å from the crystal structure (*4*)). This seems compatible with the F_X−A_1 distance of 14.8 Å, given the lateral displacement of approximately 11 Å relative to the *C*2 axis of the reaction center as indicated from other measurements (see below).

The position of A_1 was recently estimated by combining three recent spectroscopic measurements (*19*). (1) The distance from P700 to A_1 was estimated to be 25 Å, on the basis of a study of the spin-polarized $P700^+A_1^-$ radical pair (*43*). (2) The P700−A_1 vector was found to be approximately parallel to the oxygen axis of the quinone, again on the basis of simulations of the polarized radical pair (*44*).

(3) The oxygen−oxygen axis of A_1 was found to be tilted at 63° relative to the membrane (*19*). When these values are taken together with the information from the crystal structure that F_X (32 Å) is from P700 on the reaction center *C*2 axis that runs perpendicular to the membrane (*4*), then geometric constraints place A_1 at approximately 14.2 Å relative to the F_X. This is in agreement with the value measured in the present work.

From comparative and evolutionary arguments, it was suggested that A_1 occupied a position comparable to that of Q_A in the bacterial reaction center and in PSII (*45*). The crystallographic studies show that the F_X−P700 distance is 32 Å (*4*) compared to 28 Å (*46*) for the Fe−P860 distance in the bacterial reaction center; this suggests that F_X occupies a position similar to the Fe but displaced by 4 Å toward the stromal side of the membrane. If we pursue the model of PSI based on the bacterial reaction center (*45*, *4*), by moving A_1 from the "Q_A position" 3 Å toward P700 in order to comply with the distance of 25 Å for the P700-A_1 distance (*43*), then the A_1−F_X distance becomes approximately 14 Å, consistent with the distance measured here.

Overall these observations allow a model in which A_1 is found in a position that is equivalent to that of Q_A in the bacterial reaction center except for a small shift toward P700. We have recently suggested that this displacement may achieved while maintaining the ring-plane orientation close to perpendicular to the membrane plane (as found in Q_A) but allowing the oxygen−oxygen axis of the quinone to swing into the membrane until it reached an angle of at 63° to the membrane plane (*19*). Figure 7 summarizes the structural model deduced from recent spectroscopic studies.[2,3]

ACKNOWLEDGMENT

Thanks to Fraser MacMillan, Winfried Leibl, Pierre Setif, Herve Bottin, Bernard Lagoutte, Tony Matiolli, Sun Un, and Alain Boussac for useful discussion.

[2] While this paper was in preparation, an article appeared reporting spin−lattice relaxation studies of a range of PSI components including A_1^- and F_X^- (*47*). As with the present work, the authors found that F_X^- dominated the relaxation of A_1^-. However, in that work the distance between these components was calculated to be 20−30 Å, a value quite different from that reported here and one which fits poorly with other estimations in the literature. Because the relevant cw EPR spectra and kinetic traces for A_1^- were not provided, it is not possible to judge the biochemical integrity of the preparations, the quality of the data, or the goodness of the kinetic fits. Nevertheless there are two important differences between that and the present work with regard to the relaxation study of A_1^-. First, Berry et al. (*47*) studied the relaxation of A_1^- enhanced by F_X^- in the presence of reduced F_A^- and F_B^-, while in the present work we found that F_A^- and F_B^- could contaminate the A_1^- kinetics, therefore our calculation was based on data from PSI lacking F_A and F_B. Second and more importantly, Berry et al. (*47*) do not seem to have addressed the question of the *g* value of the fast relaxer (F_X^-) which is required in the equation used to calculate the distance. From the data and the calculated distance given in (*47*), we have back-calculated the *g* value used for F_X^- as approximately $g = 2$. As explained in the text this is likely to be incorrect and introduces a significant increase in the calculated distance. We specifically addressed the influence of *g* value experimentally and in our data treatment (see Materials and Methods). It seems that these two factors are sufficient to account for the discrepancy.

[3] While this paper was under review, an article appeared in which the F_X to A_1 distance was estimated indirectly as 12−16 Å (*48*). The value obtained is in excellent agreement with the present work and with the estimate obtained from our orientation studies (*19*). In addition, the position of A_1 within the PSI reaction center suggested in ref 48 is agreement with that proposed here and in ref 19.

REFERENCES

1. Golbeck, J. H. (1994) in *The Molecular Biology of Cyanobacteria* (Bryant, D. A., Ed.) pp 319.
2. Brettel, K. (1996) *Biochim. Biophys. Acta 1318*, 322.
3. Snyder, S. W., and Thurnauer, M. C. (1993) in *The Photosynthetic Reaction Centre* (Deisenhofer, J., and Norris, J. R., Eds.), Vol. 2, Academic Press: San Diego.
4. Krauss, N., Schubert, W. D., Klukas, O., Fromme, P., Witt, H. T., and Saenger, W. (1996) *Nat. Struct. Biol. 3*, 965−973.
5. Kulikov, A. V., and Likhtenstein., G. I. (1977) *Adv. Mol. Relax. Interac. Processes 10*, 47.
6. Hyde, J. S., Swartz, H. M., and Antholine, W. E (1979) in *Spin Labeling II: Theory and Applications* (Berliner, L. J., Ed.) pp 71−113, Academic Press, New York.
7. Evelo, R. G., Strying, S., Rutherford, A. W., and Hoff, A. J. (1989) *Biochim. Biophys. Acta 973*, 428.
8. Un, S., Brunel, L.-C., Brill, T. M., Zimmermann, J.-L., and Rutherford, A. W. (1994) *Proc. Nat. Acad. Sci. U.S.A. 91*, 5262.
9. Evelo, R. G., and Hoff, A. J. (1991) *J. Magn. Reson. 95*, 495.
10. Kodera, Y., Takura, K., and Kawamori A. (1992) *Biochim. Biophys. Acta 1101*, 23.
11. Hirsh, D. J., Beck, W. F., Innes, J. B., and Brudvig, G. W. (1992) *Biochemistry 31*, 532.
12. Hirsh, D. J., and Brudvig, G. W. (1993) *J. Phys. Chem. 97*, 13216.
13. Koulougliotis, D., Innes, J. B., and Brudvig, G. W. (1994) *Biochemistry 33*, 11814.
14. Koulougliotis, D., Tang, X.-S., Diner, B. A., and Brudvig, G. W. (1995) *Biochemistry 34*, 2850.
15. Deligiannakis, Y., and Rutherford, A. W. (1996) *Biochemistry*, *35*, 11239.
16. Rippka, R., Deruelles, J., Waterbury, J. B., Herdmann, M., and Stanier, R. Y. (1979*) J. Gen. Microbiol. 111*, 1−61.
17. Golbeck, J. H., Parret, K. G., Mehari, T., Jones, K. L., and Brand J. J. (1988) *FEBS Lett. 228*, 268−272.
18. Heathcote, P., Moènne-Loccoz, P., Rigby, S. E. J., and Evans, M. C. W. (1996) *Biochemistry 35*, 6644.
19. MacMillan, F., Hanley, J., van der Weerd, L., Knupling, M., Un, S., and Rutherford, A. W. (1997) *Biochemistry*, *36*, 9297.
20. Deligiannakis, Y., Boussac, A., and Rutherford, A. W. (1995) *Biochemistry 34*, 16030.
21. Dalton, L. R., Kwiram, A. L., and Cowen, L. A. (1972) *Chem. Phys. Lett. 17*, 495.
22. Beck, W. F., Innes, J. B., and Brudvig, G. W. (1990) in *Current Research in Photosynthesis* (Balschefsky, M., Ed.) p 817, Kluwer, Dordrecht.
23. Bloembergen, N. (1949) *Physica 15*, 386.
24. Abragam, A. (1961) *The Principles of Nuclear Magnetism*, Clarendon Press, Oxford.
25. Norris, J. R., Thurnauer, M. C., and Bowman, M. K. (1980) *Adv. Biol. Med. Phys. 17*, 365.
26. Rakowsky, M. H., More, M., Kulikov, A. V., Eaton, G. R., and Eaton, S. (1995) *J. Am. Chem. Soc*., *117*, 2049.
27. Bertrand, P., Guiliarelli, Gayda, J.-P., Setif, P., and Mathis, P. (1988) *Biochim. Biophys. Acta 933*, 393.
28. Goodman, G., and Leigh, J. S., Jr. (1985) *Biochemistry 24*, 2310.
29. Onishi, T., King, T. E., Salerno, J. C., Blum, H., Bowyer J. R., and Maida, T. (1981) *J. Biol. Chem. 256*, 5577.
30. Leigh, J., S., Jr. (1970) *J. Chem. Phys. 52*, 2608.
31. Golbeck, J. H., Parret, K. G., and McDermot, A. E. (1987) *Biochim. Biophys. Acta 893*, 149.
32. Goldfarb, D., and Kevan, L. (1988) *J. Magn. Reson. 76*, 276.
33. Guilliarelli, B., Guillaussier, J., More, C. Setif, P. Bottin, H., and Bertrand, P. (1993) *J. Biol. Chem. 268*, 900−908.
34. Larson, G. H., and Jeffries, C. D. (1966) *Phys. Rev. 145*, 311.
35. Gayda, J.-P., Gibson, J. F., Cammack, R., Hall, D. O., and Mullinger, R. (1976) *Biochim. Biophys. Acta 434*, 154.
36. Bowman, M. K., and Kevan, L. (1979) in *Time Domain Electron Spin Resonance* (Kevan, L., and Schwartz, R. N., Eds.) p 67, Wiley Interscience, New York.

37. Hanley, J., Deligiannakis, Y., MacMillan, F, Bottin, H., and Rutherford, A. W. (1997) *Biochemistry* 36, 11543−11549.
38. Eaton, S. S., and Eaton, G. R. (1988) *Coord. Chem. Rev. 83*, 89.
39. Moser, C. C., Keske, J. M., Warnke, K., Farid, R. S., and Dutton P. L. (1992) *Nature 355*, 796.
40. Setif, P., and Brettel, K. (1993) *Biochemistry 32*, 7846.
41. Schlodder, E., Brettel, K., Falkenberg, K., and Gergeleit, M. (1995) in *Photosynthesis: From Light to Biosphere* (Mathis, P., Ed.) Vol. 2, pp 107, Kluwer Academic Publishers, Dordrecht.
42. Leibl, W., Toupance, B., and Breton, J. (1995) *Biochemistry 34*, 10237−10244.
43. Bittl, R., and Zech, S. (1997) *J. Phys. Chem. 101*, 1429.
44. van der Est, A., Prisner, T., Bittl, R., Fromme, P. Lubitz, W., Mobius, K., and Stehlik, D. (1997) *J. Phys. Chem. 101*, 1437.
45. Nitschke, W., and Rutherford A. W. (1991) *Trends Biochem. Sci. 16*, 241−245.
46. Deisenhofer, J., and Michel, H. (1988) *EMBO J. 8*, 2149.
47. Berry, M. C., Bratt, P. J., and Evans, M. C. W. (1997) *Biochim. Biophys. Acta 1319*, 163.
48. Bittl, R., Zech, S. G., Fromme, P., Witt, H. T., and Lubitz, W. (1997) *Biochemistry 36*, 12001−12004.

BI971297P